

Signatures of α -clustering in ^{16}O by using a multiphase transport model

Yi-An Li (李逸安)^{1,2,3}, Song Zhang (张松)^{2,*} and Yu-Gang Ma (马余刚)^{2,1,†}

¹Shanghai Institute of Applied Physics, Chinese Academy of Sciences, Shanghai 201800, China

²Key Laboratory of Nuclear Physics and Ion-beam Application (MOE), Institute of Modern Physics, Fudan University, Shanghai 200433, China

³School of Nuclear Sciences and Technology, University of Chinese Academy of Sciences, Beijing 100049, China



(Received 29 May 2020; accepted 19 October 2020; published 11 November 2020)

α -clustered structures in light nuclei could be studied through “snapshots” taken by relativistic heavy-ion collisions. A multiphase transport model is employed to simulate the initial structure of collision nuclei and the proceeding collisions at center of mass energy $\sqrt{s_{NN}} = 6.37$ TeV. This initial structure can finally be reflected in the subsequent observations, such as elliptic flow (v_2), triangular flow (v_3), and quadrangular flow (v_4). Three sets of the collision systems are chosen to illustrate that the system scan is a good way to identify the exotic α -clustered nuclear structure: case I, ^{16}O nucleus (with or without α -cluster) + ordinary nuclei (always in Woods-Saxon distribution) in most central collisions; case II, ^{16}O nucleus (with or without α -cluster) + ^{197}Au nucleus collisions for centrality dependence; and case III, symmetric collision systems [namely, $^{10}\text{B} + ^{10}\text{B}$, $^{12}\text{C} + ^{12}\text{C}$, $^{16}\text{O} + ^{16}\text{O}$ (with or without α -cluster), $^{20}\text{Ne} + ^{20}\text{Ne}$, and $^{40}\text{Ca} + ^{40}\text{Ca}$] in most central collisions. Our calculations propose that relativistic heavy-ion collision experiments at $\sqrt{s_{NN}} = 6.37$ TeV are promised to distinguish the tetrahedral structure of ^{16}O from the Woods-Saxon one and shed light on the system scan projects in experiments.

DOI: [10.1103/PhysRevC.102.054907](https://doi.org/10.1103/PhysRevC.102.054907)

I. INTRODUCTION

Theoretical calculations predict that there is a new state of nuclear matter called quark-gluon plasma (QGP) created around a critical temperature $T_c \approx 170$ MeV [1,2]. In order to study the properties of this hot and dense matter, many experimental measurements have been performed at the Brookhaven National Laboratory Relativistic Heavy Ion Collider (RHIC) [3–6] as well as the CERN Large Hadron Collider (LHC), followed by many theoretical studies [7–18]. Observables such as collective flow [19–22], Hanbury Brown–Twiss (HBT) correlation [23–25], chiral electric-magnetic effects [26–32], and fluctuation [13,33] have been proposed to extract information on the properties of hot dense matter formed in these collisions. These observables can inherit information of the collision zone at very early stage (e.g., for initial nuclear geometric asymmetry). From another perspective, observables which are sensitive to initial geometry can give hints on the properties of initial state nuclei. α -clustered structure as a specific phenomenon especially in light nuclei where the mean field effect is not strong enough to break cluster structure is one of the highly interesting topics in the heavy-ion community, especially for the well-known stable nuclei ^{12}C and ^{16}O . The α -cluster model was first proposed by Gamow and later on there were extensive studies (e.g., Refs. [34–41]). However, definite α -clustered configuration of carbon and oxygen still lacks sufficient experimental evidence. Traditionally, people

believe that the nuclear structure effect is significant only in low energy nuclear collisions. However, this kind of nuclear structure phenomenon can also be manifested through relativistic heavy-ion collisions. Broniowski *et al.* [42,43] first proposed that this kind of nuclear structure phenomenon can be demonstrated through relativistic heavy-ion collisions. Observables such as harmonic flows can be measured with standard methods in relativistic heavy-ion collisions, offering a possibility to study low-energy nuclear structure phenomena at relativistic colliders, such as RHIC and LHC [44–47]. Triggered by recent experimental measurements in small systems [48–53], some theoretical works of system scan were proposed at RHIC and LHC energies by using transport models or hydrodynamics models [54–56] in which collective phenomena with respect to geometric anisotropy were discussed therein. System dependence of heavy flavor production was also calculated in Ref. [57] by using the Trento+v-USPhydro+DAB-MOD model.

This work aims at distinguishing the geometric structure of the α -clustered ^{16}O nucleus in relativistic heavy-ion collisions. From the results in this work, it is found that the participant multiplicity (N_{part}) dependence of the triangular flow over elliptic flow (v_3/v_2) can identify the exotic nuclear structure of ^{16}O via system scan studies. The rest of the paper is arranged as follows: In Sec. II a brief introduction of a multiphase transport (AMPT) model and flow analysis methods are presented. The results and discussion are presented in Sec. III, and then a summary is given.

II. MODEL AND METHODOLOGY

AMPT model is developed to describe physics in relativistic heavy-ion collisions at RHIC [58] and is also suitable to

*song_zhang@fudan.edu.cn

†mayugang@fudan.edu.cn

reproduce some results at LHC by tuning some input parameters [59], including pion-HBT correlations [60], dihadron azimuthal correlations [61,62], collective flows [55,63,64], and strangeness production [65,66]. AMPT is a hybrid dynamic transport model, which consists of four main processes: (a) the initial conditions, where the HIJING model gives the spatial and momentum distributions of minijet partons and soft string excitations; (b) partonic cascade [67], whereby interactions among partons are described by equations of motion for their Wigner distribution functions; (c) hadronization, which is conversion from the partonic to the hadronic matter; and (d) hadronic interactions, based on the a relativistic transport (ART) model [68], including baryon-baryon, baryon-meson, and meson-meson elastic and inelastic scatterings.

The initial nucleon distribution in nuclei is configured in the HIJING model [69,70] with either a pattern of Woods-Saxon distribution or where an exotic nucleon distribution is embedded to identify the α -clustered structure of ^{16}O through final state observables. For details, parameters of the tetrahedral structure of ^{16}O are inherited from an extended quantum molecular dynamics (EQMD) model [37], which is based on the quantum molecular dynamics (QMD) model. With the effective Pauli potential, the EQMD model gives reasonable α -cluster configurations for $4N$ nuclei. For four α s in the tetrahedral structure, we put them at the vertices with side length of 3.42 fm so that it gives a similar rms radius (2.699 fm) to the Woods-Saxon configuration (2.726 fm) as well as the experimental data (2.6991 fm) [71], while nucleons inside each α are initialized by using the Woods-Saxon distribution introduced in the HIJING model.

Anisotropic flow is driven by the initial anisotropic density profile in high energy heavy ion collisions and is usually characterized by complex eccentricity coefficients (ε_n) in the transverse plane as [72–74]

$$\varepsilon_n e^{in\Phi_n} \equiv -\frac{\int d^2r_\perp r^n e^{in\varphi_{\text{part}}} \rho(r, \varphi_{\text{part}})}{\int d^2r_\perp r^n \rho(r, \varphi_{\text{part}})} \equiv -\frac{\langle r^n e^{in\phi} \rangle}{\langle r^n \rangle}, \quad (1)$$

where $r = \sqrt{x^2 + y^2}$ and φ_{part} are the coordinate position and azimuthal angle of initial participant nucleons, $\rho(r, \varphi_{\text{part}})$ represents the density, and n is the order of the coefficients. Definition here is necessary but not sufficient; if we take an elliptic Gaussian distribution

$$\rho(x) = \frac{1}{2\pi\sigma_x\sigma_y} e^{-\frac{x^2}{2\sigma_x^2} - \frac{y^2}{2\sigma_y^2}}, \quad (2)$$

as an example, we expect to get zero ε_4 . However, if we calculate by the traditional definition in Eq. (1) we get nonzero value with an order of ε_2^2 . Instead, we use the cumulants [72]

$$C_4 e^{i4\Phi_4} \equiv -\frac{1}{\langle r^4 \rangle} [\langle r^4 e^{i4\phi} \rangle - 3\langle r^2 e^{i2\phi} \rangle^2], \quad (3)$$

$$\varepsilon_4^L = \varepsilon_4 + \frac{3\langle r^2 \rangle^2}{\langle r^4 \rangle} \varepsilon_2^2, \quad (4)$$

rather than moments. Although the definition is still not mathematically sufficient, it is good enough to discuss current

issues. And later we see that flow calculations have the same problem.

Eccentricities calculated by Eq. (1) are labeled as ε_2 , ε_3 , and ε_4 , and the linear part calculated by Eq. (4) is labeled as ε_4^L in the section Results and Discussion. The eccentricity calculation results of different ^{16}O structures at $\sqrt{s_{NN}} = 6.37$ TeV are plotted in Fig. 1 and are discussed later.

Usually anisotropic flows can be characterized by the Fourier decomposition of the particle azimuthal distribution in the transverse plane through the equation

$$\frac{dN}{d\varphi} \propto 1 + 2 \sum_{n=1}^{\infty} v_n \cos[n(\varphi - \Psi_n)], \quad (5)$$

where φ and Ψ_n are the azimuthal angles of final particles in momentum space and the event plane angle, respectively, and v_n is the n th-order flow coefficient. In the LHC experiments, there exists the phenomenon that the lower-order anisotropic flow v_n ($n = 2, 3$) is largely determined by a linear response to the corresponding ε_n while higher-order anisotropic flow has contributions proportional to the product of ε_2 and/or ε_3 . This can be easily understood because each order of anisotropic flow in the above equation has its own n th-order flow symmetric plane angle, and the corresponding cosine terms are not orthogonal with each other. That is to say, in principle, even for the lowest-order anisotropic flows, they have contributions from high-order ones. Fortunately, according to the experimental findings, we only need to do the simplest decomposition as follows [75–77]:

$$V_4 = V_4^{NL} + V_4^L = \chi_{4,22}(V_2)^2 + V_4^L. \quad (6)$$

The complex flow vector here is defined as $V_n \equiv v_n e^{in\Psi_n}$, where $v_n = |V_n|$ is the flow coefficient, and Ψ_n represents the azimuth of V_n in momentum space. The simplest approach to obtain v_n is using the two-particle correlations

$$v_n\{2\} = \langle \langle \cos n(\varphi_1 - \varphi_2) \rangle \rangle^{1/2} = \langle v_n^2 \rangle^{1/2}. \quad (7)$$

To suppress nonflow effects, events are divided into two subevents A and B , separated by a pseudorapidity gap, and the equation is modified as

$$v_n\{2\} = \langle \langle \cos n(\varphi_1^A - \varphi_2^B) \rangle \rangle^{1/2} = \langle v_n^2 \rangle^{1/2}, \quad (8)$$

$$v_{4,22}^A = \frac{\langle \langle \cos(4\varphi_1^A - 2\varphi_2^B - 2\varphi_3^B) \rangle \rangle}{\sqrt{\langle \langle \cos(2\varphi_1^A + 2\varphi_2^A - 2\varphi_3^B - 2\varphi_4^B) \rangle \rangle}}. \quad (9)$$

We can take the following approximation as the correlation between lower and higher flow coefficients is weak:

$$v_{4,22} = \frac{\langle v_4 v_2^2 \cos(4\Psi_4 - 4\Psi_2) \rangle}{\sqrt{\langle v_2^4 \rangle}} \approx \langle v_4 \cos(4\Psi_4 - 4\Psi_2) \rangle, \quad (10)$$

and the magnitude of the linear mode in higher-order anisotropic flows is calculated as

$$v_4^L = \sqrt{v_4^2\{2\} - v_{4,22}^2}. \quad (11)$$

This acoustic scaling of linear and mode-coupled anisotropic flow calculations is shown in Fig. 2 and discussed

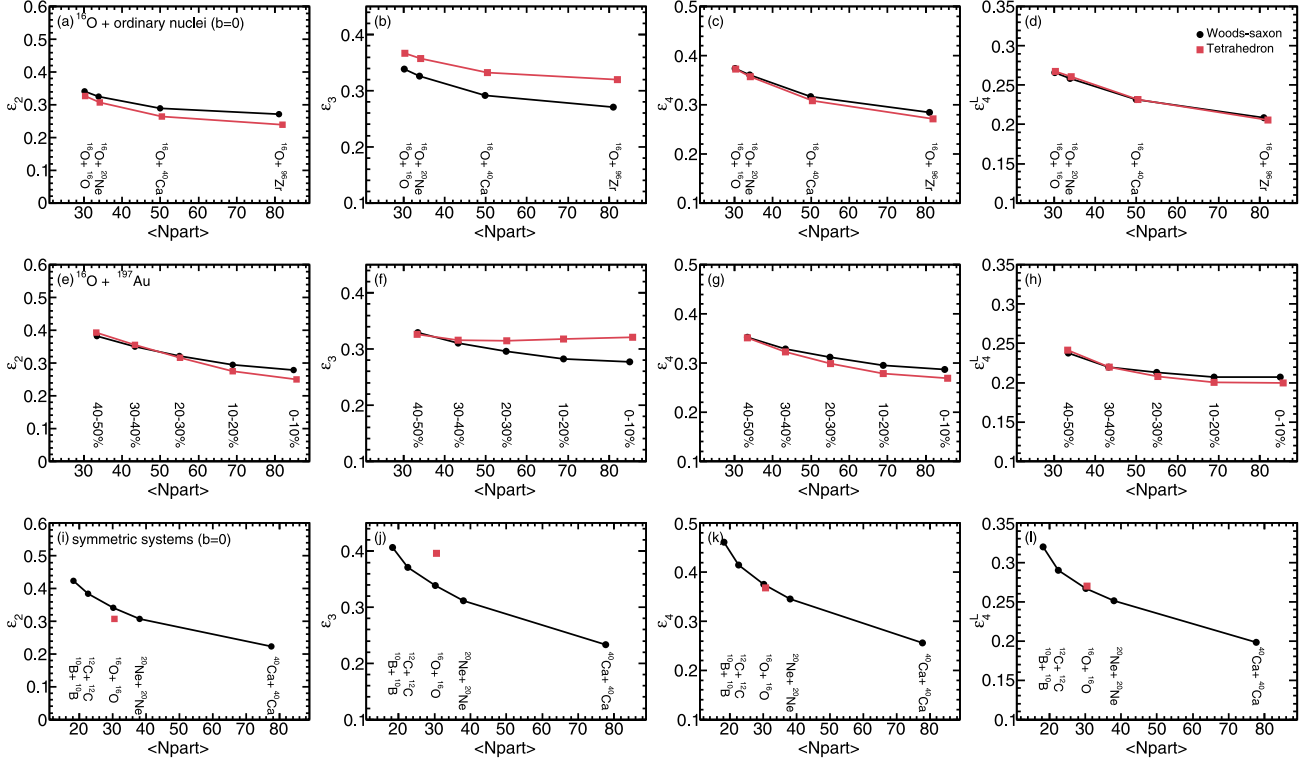


FIG. 1. Eccentricity coefficients, namely, ε_2 , ε_3 , ε_4 , and ε_4^L (from left column to right column) as a function of number of participants ($\langle N_{\text{part}} \rangle$). Top panels [case I, (a)–(d)] are the results from the most central collisions of the ^{16}O nucleus (with or without α -cluster) + ordinary nuclei (^{16}O , ^{20}Ne , ^{40}Ca , and ^{96}Zr). Middle panels [case II, (e)–(h)] are the results for the centrality dependence of the ^{16}O (with or without α -cluster) + ^{197}Au collisions. Bottom panels [case III, (i)–(l)] represent the symmetric collision systems from small to large ones in the most central collisions, i.e., $^{10}\text{B} + ^{10}\text{B}$, $^{12}\text{C} + ^{12}\text{C}$, $^{16}\text{O} + ^{16}\text{O}$ (with or without α -cluster), $^{20}\text{Ne} + ^{20}\text{Ne}$, and $^{40}\text{Ca} + ^{40}\text{Ca}$.

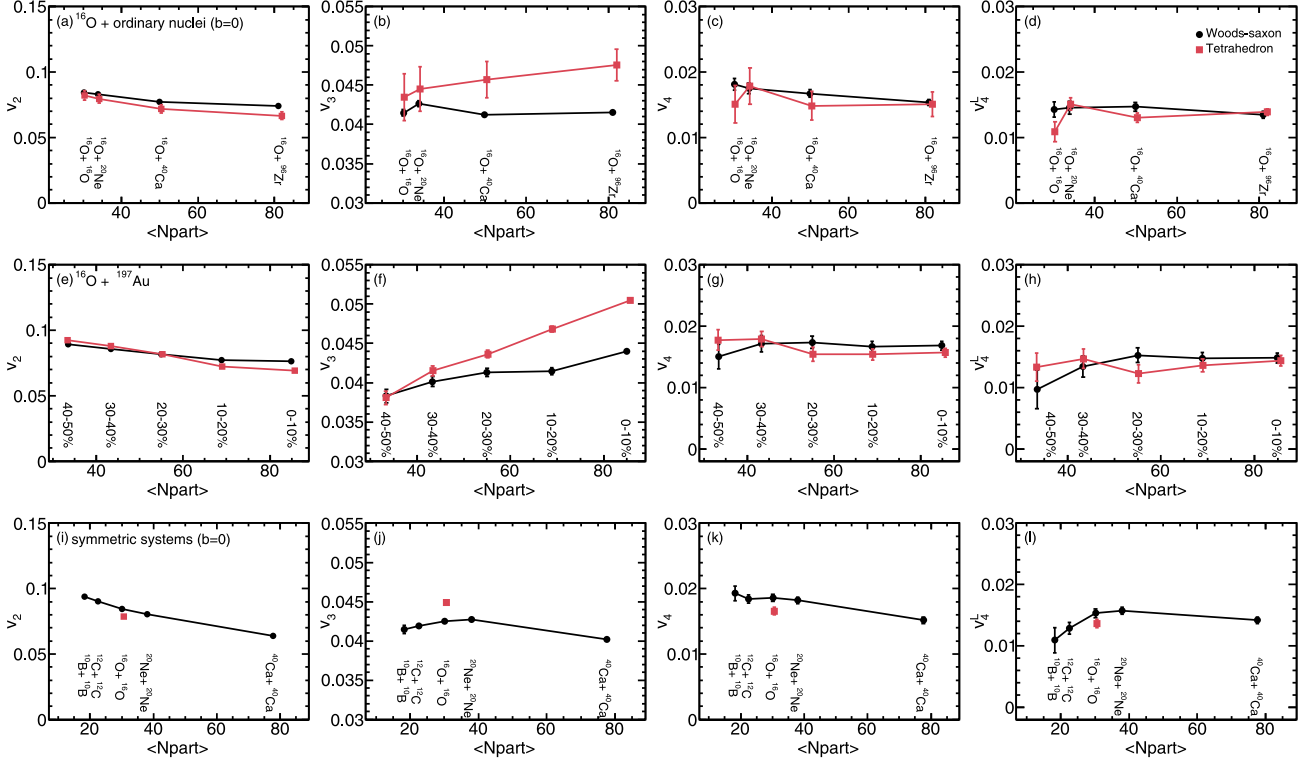
in the Results and Discussion section. To make sure that the visible qualitative results are not affected by the calculation method, we use another flow analysis with cumulants mentioned in Ref. [78] and find the qualitative conclusion is consistent.

III. RESULTS AND DISCUSSION

To investigate exotic structure of α -clustered ^{16}O , three sets of collision systems at center of mass energy $\sqrt{s_{NN}} = 6.37$ TeV are considered in this work, namely, case I, the ^{16}O nucleus (with or without α -cluster) + ordinary target nuclei inside which nucleons are always in the Woods-Saxon distribution in most central collisions ($b = 0$), and these ordinary target nuclei include ^{16}O , ^{20}Ne , ^{40}Ca , and ^{96}Zr ; case II, the centrality dependence of ^{16}O (with or without α -cluster) + ^{197}Au collisions; and case III, the symmetric collision systems from small systems to large ones, namely, $^{10}\text{B} + ^{10}\text{B}$, $^{12}\text{C} + ^{12}\text{C}$, $^{16}\text{O} + ^{16}\text{O}$ (with or without α -cluster), $^{20}\text{Ne} + ^{20}\text{Ne}$, and $^{40}\text{Ca} + ^{40}\text{Ca}$, in the most central collisions, in which nuclei except ^{16}O are calculated with the ordinary Woods-Saxon nuclear structure. In this work, we define $\langle N_{\text{part}} \rangle$ as the average number of participant nucleons in collisions, and for case II we first determine the centralities by N_{track} (number of final state charged particles) and take the last five centralities (namely, 40–50%, 30–40%, 20–30%, 10–20%,

and 0–10%) to calculate the $\langle N_{\text{part}} \rangle$ for each centrality. The eccentricity coefficients were calculated through initial partons in the AMPT model and the anisotropic flow coefficients were analyzed including charged hadrons (π^\pm , K^\pm , p , and \bar{p}) with kinetic windows for the rapidity cut ($-0.5 < y < 0.5$) and transverse momentum cut ($0.2 < p_T < 3$) GeV/c.

Figure 1 shows the eccentricity coefficients ε_n ($n = 2, 3, 4$) and ε_4^L of different collision systems (labeled with $\langle N_{\text{part}} \rangle$) at center of mass energy $\sqrt{s_{NN}} = 6.37$ TeV from left to right columns. Figures 1(a)–1(d) present ε_n ($n = 2, 3, 4$) and ε_4^L for the case mentioned above, namely, different structured ^{16}O nucleus + ordinary nuclei (^{16}O , ^{20}Ne , ^{40}Ca , ^{96}Zr) always have the Woods-Saxon nucleon distribution) in the most central collisions. In this case, ε_2 decreases with the increasing of the collision system size and the tetrahedral structure configuration presents a little higher value of ε_2 . ε_4 gives the similar system size dependence of ε_2 and ε_4^L takes approximately the same value between the patterns with different configurations of ^{16}O . ε_3 also shows the decreasing trend with system size, and in each given collision system ^{16}O in the tetrahedral structure gives larger ε_3 than that of the Woods-Saxon structure. Figures 1(e)–1(h) display centrality ($\langle N_{\text{part}} \rangle$) dependence of ε_n ($n = 2, 3, 4$) and ε_4^L in $^{16}\text{O} + ^{197}\text{Au}$ collisions, i.e., case II mentioned above. It is obvious that all ε_2 , ε_3 , and ε_4 decrease with the increasing of $\langle N_{\text{part}} \rangle$ except for the ε_3 with configuration of ^{16}O in the tetrahedral structure. The tetrahedron


 FIG. 2. Same as Fig. 1 but for anisotropic flow coefficients, namely, v_2 , v_3 , v_4 , and its linear mode v_4^L .

structure configuration of ^{16}O also presented smaller ε_2 (ε_4) and larger ε_3 than the Woods-Saxon configuration did in this case. For case III, ε_n ($n = 2, 3, 4$) and ε_4^L as a function of $\langle N_{\text{part}} \rangle$ present a downward trend for the configuration of initial nucleons in the Woods-Saxon distribution, as shown in Figs. 1(i)–1(l), respectively. The assumed α -clustered ^{16}O in the tetrahedral structure gives an obvious deviation for the eccentricity coefficients ε_3 from that of the Woods-Saxon configuration. We can see that ε_4 takes the order of ε_2 and if we subtract the contributions of ε_2 , namely, ε_4^L , the results are almost the same for different ^{16}O structures. Here we have the first conclusion: In the above collision systems, quite a large part of ε_4 is originated from the ε_2 especially for small systems, which is important for the understanding of the flow calculations shown below. We end here and do not show higher-order calculation results because the figure shows the higher-order calculation is somewhat unnecessary in small systems due to the fluctuations.

Eccentricity coefficients reflect both initial geometry distribution and initial fluctuations. In this context, the system scan project could be a potential way to distinguish the initial intrinsic geometry distribution, depending on how sensitive the final observables in momentum space, such as anisotropic flows, are to the initial geometry distribution.

Figure 2 shows the anisotropic flow coefficients v_n ($n = 2, 3, 4$) and the fourth-order linear mode v_4^L for case I, i.e., $^{16}\text{O} + \text{ordinary nuclei}$ at $b = 0$ fm, which are presented in Figs. 2(a)–2(d); case II, i.e., $^{16}\text{O} + \text{Au}$ at different centralities, which are presented in Figs. 2(e)–2(h); and case III, i.e., various symmetric collisions at $b = 0$ fm, which are presented

in Figs. 2(i)–2(l). We find that anisotropic flow coefficients present similar $\langle N_{\text{part}} \rangle$ dependence as the eccentricity coefficients. Since v_4 shows similar $\langle N_{\text{part}} \rangle$ dependence with v_2 [we can see this in Figs. 2(c), 2(g), and 2(k), and Figs. 2(a), 2(e), and 2(i)], v_2 and v_3 are discussed for distinguishing the initial geometry distribution. v_n ($n = 2, 3, 4$) from the configuration of ^{16}O in tetrahedral 4α structures are obviously deviated from the Woods-Saxon configuration as eccentricity discussed above in case III. From case III, the Woods-Saxon configuration presents a smooth $\langle N_{\text{part}} \rangle$ dependence of anisotropic flow (or eccentricity), and at the point of $\text{O} + \text{O}$ collisions, there occurs a peak or dip if ^{16}O is in a tetrahedral α -clustered structure. From cases I and II, the $\langle N_{\text{part}} \rangle$ dependence trend of v_3 can also distinguish the tetrahedral α -clustered ^{16}O from the Woods-Saxon distribution. Note that the collective flow coefficients in $^{16}\text{O} + ^{16}\text{O}$ collisions were consistent with the theoretical works [54] by using the AMPT model with nuclei of the Woods-Saxon configuration.

To further compare the three cases, the ratio of anisotropic flow coefficients v_3/v_2 was presented in Fig. 3. For case I, v_3/v_2 approximately keeps flat as a function of $\langle N_{\text{part}} \rangle$ for configurations of ^{16}O in the Woods-Saxon distribution; however, it increases with $\langle N_{\text{part}} \rangle$ for the α -clustered tetrahedral ^{16}O structure. For case II, the ratio v_3/v_2 presents an upward trend with $\langle N_{\text{part}} \rangle$ in the Woods-Saxon distribution as well as the tetrahedral configuration of ^{16}O . From cases I and II, the collision system as a “magnifier” can enlarge the ratio v_3/v_2 with the increasing of the system size. For case III, v_3/v_2 displays an $\langle N_{\text{part}} \rangle$ dependence for the Woods-Saxon distribution, and the tetrahedral configuration of ^{16}O results in an enhanced

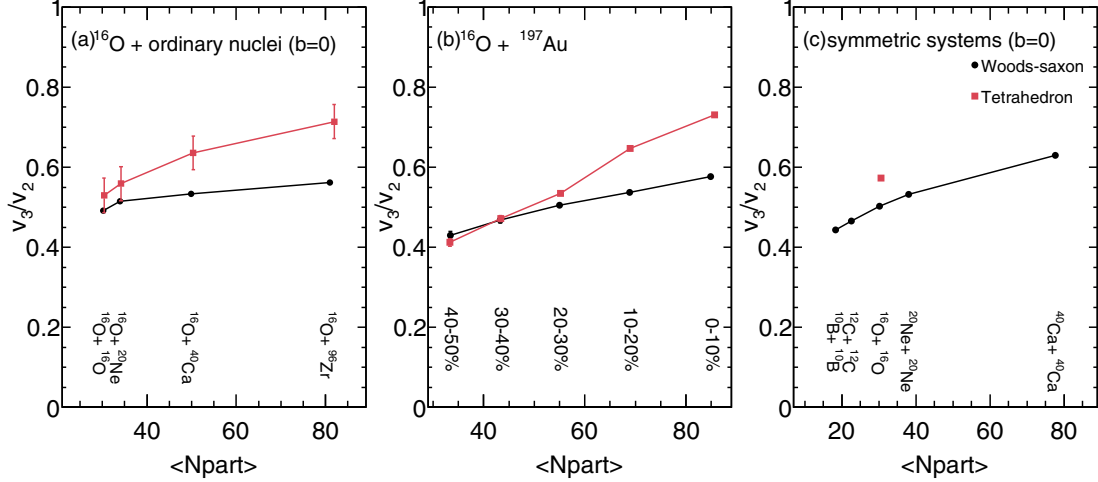


FIG. 3. Ratio v_3/v_2 as a function of $\langle N_{\text{part}} \rangle$: (a) case I, ^{16}O + ordinary nuclei at $b = 0$ fm; (b) case II, ^{16}O + Au at different centralities, and (c) case III, symmetric collisions at $b = 0$ fm. The red or black lines (symbols) represent ^{16}O with or without α -cluster structure, respectively.

point beyond the Woods-Saxon baseline. The source of initial geometry for case II, namely, centrality dependence in O + Au collisions, contains more complex components, such as nuclear intrinsic geometry, initial fluctuation, and geometry of the overlap region between target and projectile nuclei. Cases I and III are chosen in the most central collisions, which can also be achievable in experiment, to avoid the geometry distribution from the overlap region as much as possible. And from the above results and discussion, it is concluded that v_3/v_2 can be taken as a probe to identify the α -clustered structure of ^{16}O , and cases I and III are proposed as a potential scenario of a system scan experiment project at RHIC or LHC.

From the propositions of hydrodynamics [14,72,73,79–81], the relationship between initial geometry and final anisotropic flow can be described by $v_n \propto \varepsilon_n$ for lower orders $n = 2, 3$ and $v_n^L \propto \varepsilon_n^L$ for higher orders $n > 3$. These relations provide efficiency information of the transformation from initial geometry properties to final momentum space in heavy-ion collisions. Figure 4 shows the ratio v_n/ε_n ($n = 2, 3$) as well as v_4^L/ε_4^L for case I [Figs. 4(a)–4(c)], case II [Figs. 4(d)–4(f)], and case III [Figs. 4(g)–4(i)]. All ratios increase with $\langle N_{\text{part}} \rangle$ and show no significant difference between two configurations of ^{16}O . This implies the transformation efficiency is quite similar for these collision systems, and both ratios v_n/ε_n ($n = 2, 3$) and v_4^L/ε_4^L seem to only depend on the system size, such as $\langle N_{\text{part}} \rangle$ at a given center of mass energy. It is noted that the values of v_n/ε_n ($n = 2, 3$) and v_4^L/ε_4^L are related to the ratio of shear viscosity (η) over entropy density (s) of hot dense matter as pointed out in some previous studies [73,74]; the fact that the insensitivity to geometrical configuration of v_2/ε_2 , v_3/ε_3 , and v_4^L/ε_4^L in the present calculation in turn provides us the possibility to extract η/s if the suitable viscous hydrodynamics model is used also indicates that η/s might be insensitive to the initial geometric structure. However, due to the canceling-out effect of η/s , the v_3/v_2 will be a good probe to identify the geometric structure regardless of the η/s .

Finally, to give an illustrative interpretation for v_3 's sensitivity to the geometric structure, we consider to project the

^{16}O nucleus into the transverse plane after a three-dimensional rotation, where there will be a larger probability to see some projected images due to its high structural symmetry. Take the tetrahedral structure, for an example. If we draw the projection of participant nucleons in the initial collision or the density distribution of partons in the HIJING procedure, it is more likely that one would observe triangular images rather than that of the Woods-Saxon structure, which results in large triangularity flow v_3 . Besides that, fluctuation in small systems also plays an important role in the final state. With increasing of the system size, fluctuation becomes weaker and the intrinsic geometry will contribute more to the eccentricity coefficients and then the final collective flow. Therefore, the collision system dependence of final observables which are sensitive to initial geometry properties can indicate the intrinsic geometry distribution and then can be taken as a probe to distinguish the α -clustering nuclear structure.

IV. SUMMARY

In summary, the present study shows the AMPT calculations of anisotropic flows in relativistic heavy ion collisions including ^{16}O which is assumed to have exotic tetrahedral structure with four α -clusters. Three different sets of system scans at center of mass energy $\sqrt{s_{NN}} = 6.37$ TeV were considered. Case I is the ordinary structured target size scan by the different configured ^{16}O projectile in the most central collisions, case II presents the centrality scan for $^{16}\text{O} + ^{197}\text{Au}$ collisions, and case III describes the symmetric collision system scan (namely, B + B, C + C, O + O, Ne + Ne, and Ca + Ca) in the most central collisions. From the systematic calculation results of the above three cases, it demonstrates that v_3 , v_2 , and the ratio v_3/v_2 can be taken as a powerful probe to distinguish the tetrahedral configuration of ^{16}O from the Woods-Saxon configuration in the ground state. And the collision systems for case I and case III are proposed to be the system scan experiment projects at RHIC or LHC.

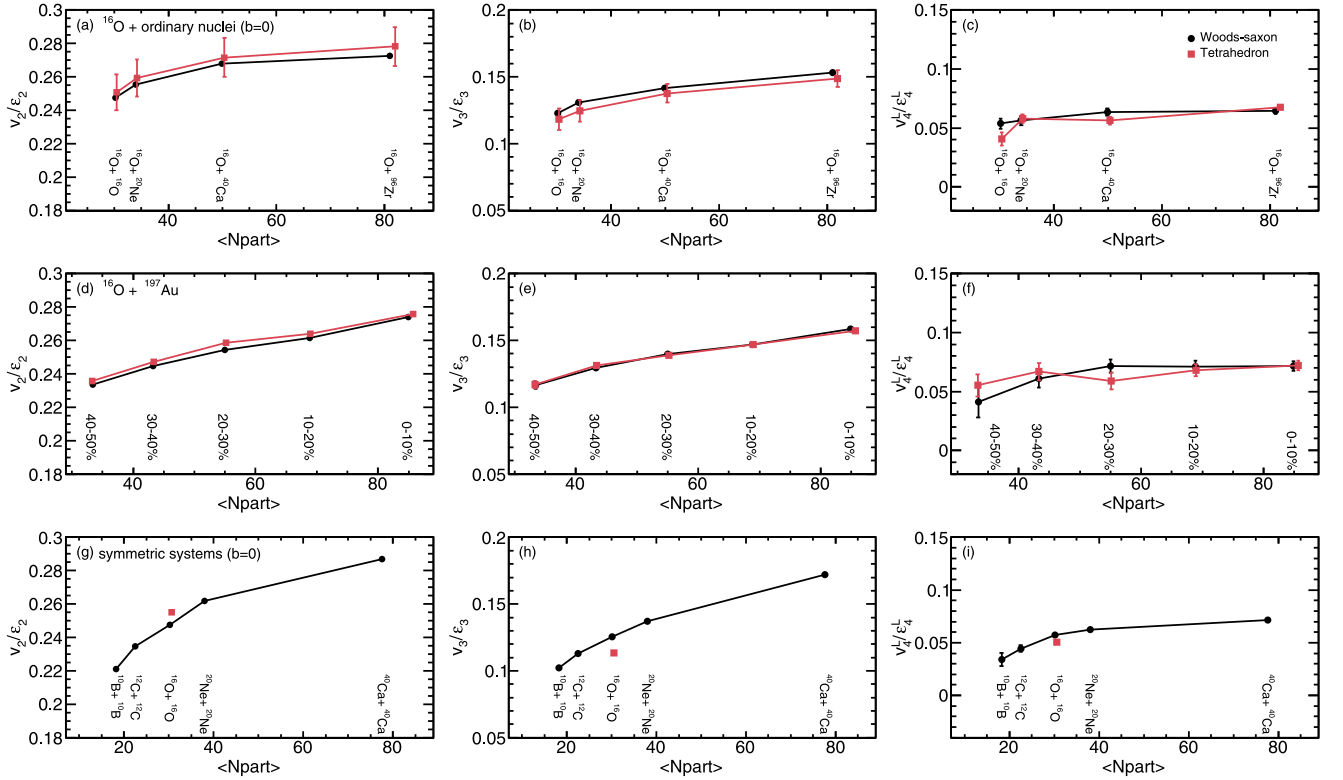


FIG. 4. Ratios v_2/ε_2 (left column), v_3/ε_3 (middle column), and v_4^L/ε_4^L (right column) as a function of number of participants $\langle N_{\text{part}} \rangle$. Top row [(a)–(c)]: case I, ^{16}O + ordinary nuclei at $b = 0$ fm. Middle row [(d)–(f)]: case II, ^{16}O + Au at different centralities. Bottom row [(g)–(i)]: case III, symmetric collisions at $b = 0$ fm. The red or black lines (symbols) represent ^{16}O with or without α -cluster structure, respectively.

ACKNOWLEDGMENTS

This work was supported in part by the National Natural Science Foundation of China under Contracts No. 11890714, No. 11875066, No. 11421505, No. 11961141003, and No. 11935001 and the National Key R&D Program of China under

Grants No. 2016YFE0100900 and No. 2018YFE0104600, the Strategic Priority Research Program of the CAS under Grants No. XDB34030200 and No. XDB16, and the Key Research Program of Frontier Sciences of the CAS under Grant No. QYZDJ-SSW-SLH002.

- [1] Y. Aoki, S. Borsanyi, S. Drr, Z. Fodor, S. D. Katz, S. Krieg, and K. Szabo, *J. High Energy Phys.* **06** (2009) 088.
- [2] A. Bazavov, T. Bhattacharya, M. Cheng, C. DeTar, H.-T. Ding, S. Gottlieb, R. Gupta, P. Hegde, U. M. Heller, F. Karsch *et al.* (HotQCD Collaboration), *Phys. Rev. D* **85**, 054503 (2012).
- [3] I. Arsene *et al.* (BRAHMS Collaboration), *Nucl. Phys. A* **757**, 1 (2005).
- [4] B. Back, M. Baker, M. Ballintijn, D. Barton, B. Becker, R. Betts, A. Bickley, R. Bindel, A. Budzanowski, W. Busza *et al.*, *Nucl. Phys. A* **757**, 28 (2005).
- [5] J. Adams, M. Aggarwal, Z. Ahammed, J. Amonett, B. Anderson, D. Arkhipkin, G. Averichev, S. Badyal, Y. Bai, J. Balewski *et al.*, *Nucl. Phys. A* **757**, 102 (2005).
- [6] K. Adcox, S. Adler, S. Afanasiev, C. Aidala, N. Ajitanand, Y. Akiba, A. Al-Jamel, J. Alexander, R. Amirkas, K. Aoki *et al.*, *Nucl. Phys. A* **757**, 184 (2005).
- [7] J. L. Nagle and W. A. Zajc, *Annu. Rev. Nucl. Part. Sci.* **68**, 211 (2018).
- [8] P. Braun-Munzinger, V. Koch, T. Schafer, and J. Stachel, *Phys. Rep.* **621**, 76 (2016).
- [9] J. Chen, D. Keane, Y.-G. Ma, A. Tang, and Z. Xu, *Phys. Rep.* **760**, 1 (2018).
- [10] A. Bzdak, S. Esumi, V. Koch, J. Liao, M. Stephanov, and N. Xu, *Phys. Rep.* **853**, 1 (2020).
- [11] A. Andronic, P. Braun-Munzinger, K. Redlich, and J. Stachel, *Nature* **561**, 321 (2018).
- [12] F. G. Gardim, G. Giacalone, M. Luzum, and J.-Y. Ollitrault, *Nat. Phys.* **16**, 615 (2020).
- [13] X. Luo and N. Xu, *Nucl. Sci. Tech.* **28**, 112 (2017).
- [14] H. Song, Y. Zhou, and K. Gajdosova, *Nucl. Sci. Tech.* **28**, 99 (2017).
- [15] Y. G. Ma, *Sci. Sin. Phys. Mech. Astron.* **49**, 102001 (2019).
- [16] H. L. Lao, F. H. Liu, B. C. Li, M.-Y. Duan, and R. A. Lacey, *Nucl. Sci. Tech.* **29**, 164 (2018).
- [17] H.-L. Lao, F.-H. Liu, B.-C. Li, and M.-Y. Duan, *Nucl. Sci. Tech.* **29**, 82 (2018).
- [18] H.-M. Wang, Z.-Y. Hou, X.-T. Wang, and X.-J. Sun, *Nucl. Sci. Tech.* **29**, 116 (2018).
- [19] L. Adamczyk, J. K. Adkins, G. Agakishiev, M. M. Aggarwal, Z. Ahammed, I. Alekseev, J. Alford, C. D. Anson, A. Aparin, D. Arkhipkin *et al.* (STAR Collaboration), *Phys. Rev. C* **88**, 014902 (2013).
- [20] L. Adamczyk, J. K. Adkins, G. Agakishiev, M. M. Aggarwal, Z. Ahammed, I. Alekseev, J. Alford, C. D. Anson, A. Aparin,

- D. Arkhipkin *et al.* (STAR Collaboration), *Phys. Rev. Lett.* **112**, 162301 (2014).
- [21] L. Adamczyk, J. K. Adkins, G. Agakishiev, M. M. Aggarwal, Z. Ahammed, A. V. Alakhverdyants, I. Alekseev, J. Alford, C. D. Anson, D. Arkhipkin *et al.* (STAR Collaboration), *Phys. Rev. C* **88**, 014904 (2013).
- [22] L. Adamczyk, J. K. Adkins, G. Agakishiev, M. M. Aggarwal, Z. Ahammed, I. Alekseev, J. Alford, A. Aparin, D. Arkhipkin, E. C. Aschenauer *et al.* (STAR Collaboration), *Phys. Rev. Lett.* **114**, 252302 (2015).
- [23] L. Adamczyk, J. K. Adkins, G. Agakishiev, M. M. Aggarwal, Z. Ahammed, I. Alekseev, J. Alford, C. D. Anson, A. Aparin, D. Arkhipkin *et al.* (STAR Collaboration), *Phys. Rev. C* **92**, 014904 (2015).
- [24] A. Adare, S. Afanasiev, C. Aidala, N. N. Ajitanand, Y. Akiba, R. Akimoto, H. Al-Bataineh, H. Al-Ta'ani, J. Alexander, M. Alfred *et al.*, [arXiv:1410.2559](https://arxiv.org/abs/1410.2559).
- [25] R. A. Lacey, *Phys. Rev. Lett.* **114**, 142301 (2015).
- [26] D. Kharzeev, J. Liao, S. Voloshin, and G. Wang, *Prog. Part. Nucl. Phys.* **88**, 1 (2016).
- [27] K. Fukushima, *Prog. Part. Nucl. Phys.* **107**, 167 (2019).
- [28] G.-L. Ma and X.-G. Huang, *Phys. Rev. C* **91**, 054901 (2015).
- [29] Y. C. Liu and X.-G. Huang, *Nucl. Sci. Tech.* **31**, 56 (2020).
- [30] F. Q. Wang and J. Zhao, *Nucl. Sci. Tech.* **29**, 179 (2018).
- [31] Z.-W. Xu, S. Zhang, Y.-G. Ma, J.-H. Chen, and C. Zhong, *Nucl. Sci. Tech.* **29**, 186 (2018).
- [32] J.-H. Gao, G.-L. Ma, S. Pu, and Q. Wang, *Nucl. Sci. Tech.* **31**, 90 (2020).
- [33] L. Adamczyk, J. K. Adkins, G. Agakishiev, M. M. Aggarwal, Z. Ahammed, I. Alekseev, J. Alford, A. Aparin, D. Arkhipkin, E. C. Aschenauer *et al.* (STAR Collaboration), *Phys. Rev. C* **92**, 021901 (2015).
- [34] J. A. Wheeler, *Phys. Rev.* **52**, 1083 (1937).
- [35] L. R. Hafstad and E. Teller, *Phys. Rev.* **54**, 681 (1938).
- [36] W. von Oertzen, M. Freer, and Y. Kanada-En'yo, *Phys. Rep.* **432**, 43 (2006).
- [37] W. B. He, Y. G. Ma, X. G. Cao, X. Z. Cai, and G. Q. Zhang, *Phys. Rev. Lett.* **113**, 032506 (2014).
- [38] W. B. He, Y. G. Ma, X. G. Cao, X. Z. Cai, and G. Q. Zhang, *Phys. Rev. C* **94**, 014301 (2016).
- [39] B. S. Huang, Y. G. Ma, and W. B. He, *Phys. Rev. C* **95**, 034606 (2017).
- [40] B.-S. Huang and Y.-G. Ma, *Phys. Rev. C* **101**, 034615 (2020).
- [41] Y. Liu and Y.-L. Ye, *Nucl. Sci. Tech.* **29**, 184 (2018).
- [42] W. Broniowski and E. Ruiz Arriola, *Phys. Rev. Lett.* **112**, 112501 (2014).
- [43] P. Bożek, W. Broniowski, E. R. Arriola, and M. Rybczyński, *Phys. Rev. C* **90**, 064902 (2014).
- [44] W. Broniowski, P. Bożek, M. Rybczyński, and E. R. Arriola, *Acta Phys. Pol. B Proc. Suppl.* **8**, 301 (2015).
- [45] M. Rybczyński, M. Piotrowska, and W. Broniowski, *Phys. Rev. C* **97**, 034912 (2018).
- [46] M. Rybczyński and W. Broniowski, *Phys. Rev. C* **100**, 064912 (2019).
- [47] S. Zhang, Y. G. Ma, J. H. Chen, W. B. He, and C. Zhong, *Phys. Rev. C* **95**, 064904 (2017).
- [48] A. Adare, C. Aidala, N. N. Ajitanand, Y. Akiba, M. Alfred, V. Andrieux, K. Aoki, N. Apadula, H. Asano, C. Ayuso *et al.* (PHENIX Collaboration), *Phys. Rev. Lett.* **121**, 222301 (2018).
- [49] C. Aidala *et al.* (PHENIX Collaboration), *Nat. Phys.* **15**, 214 (2019).
- [50] S. Huang (for STAR Collaboration), *Nucl. Phys. A* **982**, 475 (2019).
- [51] S. Chatrchyan *et al.* (CMS Collaboration), *Phys. Lett. B* **718**, 795 (2013).
- [52] G. Aad *et al.* (ATLAS Collaboration), *Phys. Rev. Lett.* **116**, 172301 (2016).
- [53] J. Adam *et al.* (ALICE Collaboration), *Nat. Phys.* **13**, 535 (2017).
- [54] S. H. Lim, J. Carlson, C. Loizides, D. Lonardon, J. E. Lynn, J. L. Nagle, J. D. Orjuela Koop, and J. Ouellette, *Phys. Rev. C* **99**, 044904 (2019).
- [55] S. Huang, Z. Chen, W. Li, and J. Jia, *Phys. Rev. C* **101**, 021901 (2020).
- [56] M. Sievert and J. Noronha-Hostler, *Phys. Rev. C* **100**, 024904 (2019).
- [57] R. Katz, C. A. G. Prado, J. Noronha-Hostler, and A. A. P. Suaide, *Phys. Rev. C* **102**, 041901(R) (2020).
- [58] Z.-W. Lin, C. M. Ko, B.-A. Li, B. Zhang, and S. Pal, *Phys. Rev. C* **72**, 064901 (2005).
- [59] G.-L. Ma and Z.-W. Lin, *Phys. Rev. C* **93**, 054911 (2016).
- [60] Z.-w. Lin, C. M. Ko, and S. Pal, *Phys. Rev. Lett.* **89**, 152301 (2002).
- [61] G.-L. Ma *et al.*, *Phys. Lett. B* **641**, 362 (2006).
- [62] H. Wang, J. H. Chen, Y. G. Ma, and S. Zhang, *Nucl. Sci. Tech.* **30**, 185 (2019).
- [63] B. I. Abelev *et al.* (STAR Collaboration), *Phys. Rev. Lett.* **101**, 252301 (2008).
- [64] A. Bzdak and G.-L. Ma, *Phys. Rev. Lett.* **113**, 252301 (2014).
- [65] X.-H. Jin, J.-H. Chen, Y.-G. Ma, S. Zhang, C.-J. Zhang, and C. Zhong, *Nucl. Sci. Tech.* **29**, 54 (2018).
- [66] X.-H. Jin, J.-H. Chen, Z. Lin, G.-L. Ma, Y.-G. Ma, and S. Zhang, *Sci. China: Phys., Mech. Astron.* **62**, 11012 (2019).
- [67] B. Zhang, *Comput. Phys. Commun.* **109**, 193 (1998).
- [68] B.-A. Li and C. M. Ko, *Phys. Rev. C* **52**, 2037 (1995).
- [69] X.-N. Wang and M. Gyulassy, *Phys. Rev. D* **44**, 3501 (1991).
- [70] M. Gyulassy and X.-N. Wang, *Comput. Phys. Commun.* **83**, 307 (1994).
- [71] I. Angeli and K. Marinova, *At. Data Nucl. Data Tables* **99**, 69 (2013).
- [72] D. Teaney and L. Yan, *Phys. Rev. C* **86**, 044908 (2012).
- [73] P. Liu and R. A. Lacey, *Phys. Rev. C* **98**, 021902 (2018).
- [74] S. Zhang, Y. G. Ma, G. L. Ma, J. H. Chen, Q. Shou, W. He, and C. Zhong, *Phys. Lett. B* **804**, 135366 (2020).
- [75] L. Yan and J.-Y. Ollitrault, *Phys. Lett. B* **744**, 82 (2015).
- [76] G. Aad, B. Abbott, J. Abdallah, O. Abdinov, R. Aben, M. Abolins, O. S. AbouZeid, H. Abramowicz, H. Abreu, R. Abreu *et al.* (ATLAS Collaboration), *Phys. Rev. C* **92**, 034903 (2015).
- [77] S. Acharya, D. Adamová, J. Adolfsson, M. Aggarwal, G. A. Rinella, M. Agnello, N. Agrawal, Z. Ahammed, N. Ahmad, S. Ahn *et al.*, *Phys. Lett. B* **773**, 68 (2017).
- [78] N. Borghini, P. M. Dinh, and J.-Y. Ollitrault, *Phys. Rev. C* **64**, 054901 (2001).
- [79] F. G. Gardim, F. Grassi, M. Luzum, and J.-Y. Ollitrault, *Phys. Rev. C* **85**, 024908 (2012).
- [80] H. Niemi, G. S. Denicol, H. Holopainen, and P. Huovinen, *Phys. Rev. C* **87**, 054901 (2013).
- [81] R. S. Bhalerao, J.-Y. Ollitrault, and S. Pal, *Phys. Lett. B* **742**, 94 (2015).